 doi:10.20944/preprints202205.0176.v1

Article

Experimental Investigations of the Behavior of Stiffened Perforated Cold-Formed Steel Sections Subjected to Axial Compression

Fattouh M. F. Shaker [1], Zekriat Mamdooh [1] , Ahmed Deifalla [2,*] and Mohamed M. Yehia [1]

[1] Civil Eng. Department, Faculty of Eng. Mataria, Helwan University, Cairo, Egypt; fatouhm@hotmail.com, Zekriat.mamdooh@gmail.com
[2] Structural engineering and construction management department; ahmed.deifalla@fue.edu.eg
* Correspondence: ahmed.deifalla@fue.edu.eg; diffalaf@mcmaster.ca.

Abstract: The cold-formed steel sections are becoming popular for different steel structures because it has a high resistance against the different straining actions with minimum weight compared with hard steel sections. Recently, the perforated cold-formed steel (PCFS) sections are used in many applications such as storage perforated uprights racks. Experimental research into the behaviour of steel storage rack uprights subjected to axial compression is presented in this paper. The material qualities of cold-formed steel uprights were determined by tensile tests. The seventeen perforated specimens were examined under axial compression, with five different cross-sections, three different web heights and thicknesses, and varying lengths. The study's goals are to find out how perforations affect the performance and failure mode of steel storage rack uprights, discuss the interaction of distortional and global buckling, and verify the accuracy of using the Direct Strength Method (DSM) for predicting the ultimate strength of uprights failing in buckling interactions for perforated uprights. It is found that the failure modes of perforated specimens with stiffeners generally cannot be well predicted by the Direct Strength Method. But when the modifications proposed by Xianzhong Zhao etc. al. are used, their accuracy is acceptable.

Keywords: cold-formed steel; stiffened; perforation; steel racking systems; axial compression test; ultimate capacity; experimental investigation

1. Introduction

Because cold-formed steel sections can be used efficiently as structural members of lightweight structures when a hot-roll is not optimum and efficient, it is widely used in commercial, residential, and industrial constructions. It is used as component elements in steel industrial storage rack systems, such as steel uprights, beams, and bracings. In recent years the use of industrial storage rack systems is growing. Therefore, it is vital to broaden the scope of research into the structural behaviour of their elements. Upright members used in storage racking generally have many perforations. Perforations run the length of the perforated uprights, allowing the beam to be linked at different heights and the bracing to be bolted together to form the frames. Several experimental studies [1-12] have been conducted to examine the behaviour of perforated uprights to determine its load capacity.

Casafont M. et. al. [1] carried out an experimental study of steel storage rack uprights subjected to axial compression to study the failure due to modes of combination between distortional buckling and global buckling. They found that the combination of the two different modes of buckling affects the column strength and should be considered in the design. Zhao et. al. [2] presented an experimental investigation to study the structural behavior and the failure modes of 67 uprights with and without perforations subjected to axial compression. Because the Direct Strength Method (DSM) does not account for the effect of perforations, the experimental findings showed that the DSM forecasts overstated

 doi:10.20944/preprints202205.0176.v1

the load capacity. Therefore, depending on the results of the experimental study they proposed a modified (DSM) for perforated uprights. The influence of varied designs of numerous circular holes on the compressive capacity of channels was investigated by Rhodes and Schneider [3]. They carried out a series of compression experimental experiments analyzing perforation patterns. The test findings clearly reveal that the impacts of perforations on member load capacity are dependent on perforation location and size.

Crisan et al. [4] investigated the interactive buckling of steel pallet racks as compression members, with the goal of observing distortionary–global interaction and determining the ultimate strength of upright members. They studied two groups of upright members with two different cross-sections, one having perforations and the other without. They claimed that all testing was conducted in accordance with the Euro-Code for racking systems EN15512 [5] guidelines and conditions. The buckling curve for a specific type of section was calculated based on the experimental data. The experimental results led to obtaining the buckling curve for a given type of section. Roure et al. [6] conducted a comprehensive set of experimental testing on twenty different pallet-rack upright steel profiles with various cross-sections that were compressed. They compared the experimental results to the results of two different methods: analytical using the European Standard, and numerical using finite element (F.E) analysis. They discovered that while none of the methods can completely replace experimental testing and that physical testing is still required, finite element analysis can reduce the number of tests required because it reproduces the majority of the factors involved in the problem. Stub column tests were performed by K.S. Sivakumaran [7] to determine the ultimate compression strength of perforated cold-formed sections. He explained that as the diameter of the hole grew larger, the strength of these parts dropped. When analysing the effect of web holes on stub column ultimate strength, similar results have been found [8-9]. Baldassino, N et al. [10] studied the distortional buckling of cold-formed steel storage rack sections including perforations. Kwon et al. [11] studied the ultimate strength of stub and intermediate-length columns by conducting compression tests on cold-formed steel-lipped channel sections and channel sections with intermediate stiffeners at the flanges and web. Local buckling and distortional buckling happened simultaneously only for the stub columns, while the interaction between local buckling and overall buckling was the final failure mode for the intermediate and long columns. The findings of experimental tests on 36 columns with and without perforations with complicated edge stiffeners exposed to axial compression were presented by Xiang, Zhou, and Shi [12]. They found that the properties of perforations affect the ultimate strength and the deformed shape of columns.

The Direct Strength Method (DSM) was proposed by Schafer and Pekoz [13], and it has been modified over time. As an alternative design technique for cold-formed steel structures, the DSM is currently officially incorporated in the latest versions of the North American specification AISI-S100 [14] and the Australian/New Zealand standard AS/NZS4600 [15]. The DSM is recommended for its calculation efficiency, notably for design strength predictions of cold-formed steel sections with complicated stiffeners because effective section calculation is no longer needed in the design strength predictions. Many researchers studied the elastic buckling stress of perforated plates and members such as Moen and Schafer [16]. They devised simpler procedures for approximating the global, distortional, and local critical elastic buckling loads of cold-formed steel columns and beams with holes based on theoretical and FE research. Yao et al. [17] employed FE analysis to develop an effective method represent a modification of the DSM for calculating the elastic distortional buckling stress of perforated parts under axial compression.

From a careful review of the recent research on the (CFS) upright members, it is noted that they focus on studying the behavior and efficiency of these elements under the influence of the different cross-sections, perforated or non-perforated, and stiffened or non-stiffened. Most of the research on (PCFS) upright members focused on circular shape openings or slots because the method of assembling the beams to upright members in the steel racking systems was previously done using bolts. But now the assembly system has

Preprints (www.preprints.org) | NOT PEER-REVIEWED | Posted: 13 May 2022 doi:10.20944/preprints202205.0176.v1

been introduced in the manner of interlock, which calls for the presence of openings in triangular shapes. Therefore, the aims of this research are:

a. Studying experimentally the presence of triangular openings on the behavior and capacity of columns (PCFS) upright members stiffened or non-stiffened.

b. Studying the applicability of using the Direct Strength Method (DSM) to evaluate the efficiency of these sections as well as the sort of buckling that causes the collapse.

So that, the seventeen (PCFS) upright members stiffened and non-stiffened with different dimensions subjected to axial compression were tested experimentally and the results were used to achieve the objectives of this research.

2. Experimental Program

2.1. Specimens

The seventeen stiffened (PCFS) upright members were categorized into five types of cross-sections according to the web height and thickness as listed in Table (1). The specimens were labeled to specify the section type: for example, the label "C70-63.5-1.5-P-500" where "C" refers to "C-section" and the numbers following "C" refer to the overall web height (hw) of 70 mm, flange width (bf) of 63.5 mm, the thickness of section (t) of 1.5 mm and specimen length (L) of 500 mm, respectively. The letter "P" indicates that the specimen is perforated. Figure (1) shows the properties of the perforations at the web and flanges, such as shapes, locations, and dimensions, and the cross-sectional geometry of the tested specimens.

2.2. Material properties

To determine the material properties of the tested specimens, a series of tensile tests were conducted on three categories of slices with different three thicknesses (1.5, 2.0, and 2.5mm) by using a hydraulic MTS (Material Test System). Nine slices were tested for each thickness. Three of them were tacked as non-perforated flat coupons which were cut longitudinally from flat parts of the uprights, three other flat coupons with circular perforations were cut from the flanges of the uprights and the last three flat coupons with a sequence of triangular and circular perforations were cut from the webs of the uprights. The yield stress for each slice is calculated by dividing the value of its yield load according to the tensile test by the value of its net cross-section area and then the yield stress for each thickness is calculated from the average of yield stresses for the nine slices as shown in Table 2.

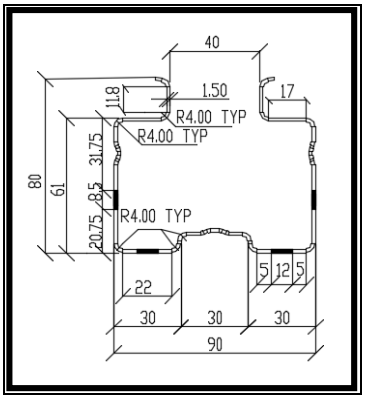

(a) Section Dimensions C70-63.5-1.5-P

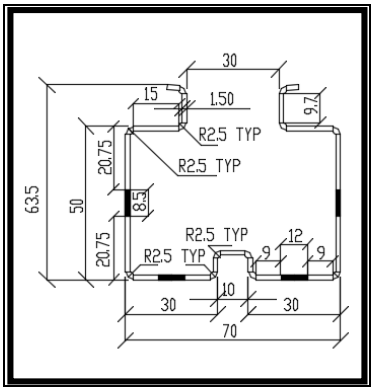

(b) Section Dimensions C90-80-1.5-P

Preprints (www.preprints.org) | NOT PEER-REVIEWED | Posted: 13 May 2022 doi:10.20944/preprints202205.0176.v1

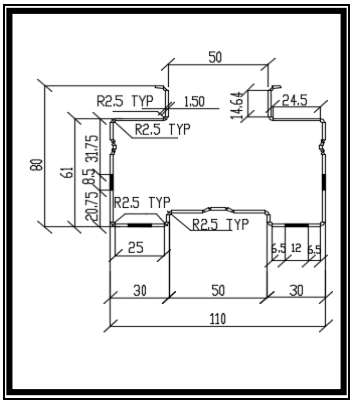

(c) Section Dimensions C110-80-1.5-P

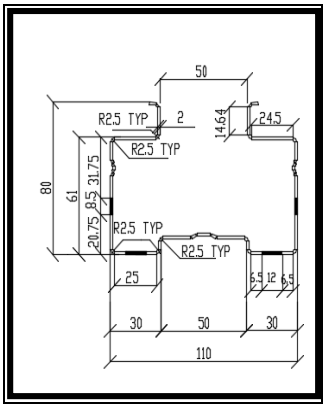

(d) Section Dimensions C110-80-2-P

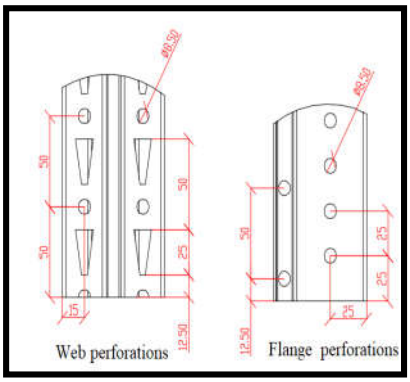

(e) Section Dimensions C110-80-2.5-P

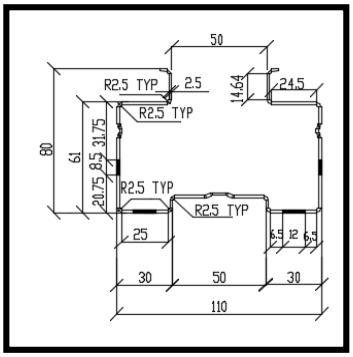

(f) Dimensions of perforations in web and flanges

Figure 1. Cross-section geometries and dimensions of the tested specimens.

Preprints (www.preprints.org) | NOT PEER-REVIEWED | Posted: 13 May 2022 doi:10.20944/preprints202205.0176.v1

Table 1. Properties of tested specimens.

Specimen	h_w (mm)	b_f (mm)	t (mm)	Length L (mm)	A_g (mm^2)	A_{net} (mm^2)	rx (net) (mm)	ry (net) (mm)	λ_x	λ_y	λ_{max}
C70-63.5-1.5-P-500	70	50	1.5	500	370.72	323.02	22.34	26.14	22.38	19.12	22.38
C70-63.5-1.5-P-1000	70	50	1.5	1000	370.72	323.02	22.34	26.14	44.76	38.25	44.76
C70-63.5-1.5-P-2000	70	50	1.5	2000	370.72	323.02	22.34	26.14	89.52	76.5	89.52
C90-80-1.5-P-500	90	80	1.5	500	455.35	407.65	27.01	33.80	18.51	14.79	18.51
C90-80-1.5-P-1000	90	80	1.5	1000	455.35	407.65	27.01	33.80	37.02	29.59	37.02
C90-80-1.5-P-1500	90	80	1.5	1500	455.35	407.65	27.01	33.80	55.54	44.38	55.54
C110-80-1.5-P-500	110	80	1.5	500	510.91	463.21	26.96	40.89	18.54	12.22	18.54
C110-80-1.5-P-1000	110	80	1.5	1000	510.91	463.21	26.96	40.89	37.09	24.45	37.09
C110-80-1.5-P-1500	110	80	1.5	1500	510.91	463.21	26.96	40.89	55.63	36.68	55.63
C110-80-1.5-P-2000	110	80	1.5	2000	510.91	463.21	26.96	40.89	74.18	48.91	74.18
C110-80-2-P-500	110	80	2	500	678.36	614.76	26.87	40.60	18.61	12.32	18.61
C110-80-2-P-1000	110	80	2	1000	678.36	614.76	26.87	40.60	37.22	24.63	37.22
C110-80-2-P-1500	110	80	2	1500	678.36	614.76	26.87	40.60	55.82	36.95	55.82
C110-80-2-P-2000	110	80	2	2000	884.34	614.76	26.87	40.60	74.43	49.26	74.43
C110-80-2.5-P-500	110	80	2.5	500	884.34	764.91	26.78	40.31	18.67	12.40	18.67
C110-80-2.5-P-1000	110	80	2.5	1000	884.34	764.91	26.78	40.31	37.34	24.81	37.34
C110-80-2.5-P-2000	110	80	2.5	2000	884.34	764.91	26.78	40.31	74.68	49.62	74.68

Table 2. The average mechanical properties of the tensile coupon test results.

Thickness of material, t (mm)	Non-perforated coupon			coupon has circular perforations from flange			coupon has triangular perforations from web			Final material properties		
	F_y (MPa)	F_u (MPa)	E (GPa)	F_y (MPa)	F_u (MPa)	E (GPa)	F_y (MPa)	F_u (MPa)	E (GPa)	F_y (MPa)	F_u (MPa)	E (GPa)
1.50	377	480	203.8	389	488	204.1	399	490	204.2	388	486	204.1
2.00	386	485	203.5	401	493	203.9	410	496	204.0	399	491	203.8
2.50	387	487	204.0	402	495	204.1	412	500	204.2	400	494	204.1

2.3. Test setup and instrumentations.

The frame consisted of a horizontal I-beam connected with bolted rigid connection to two vertical columns. The frame rested on the floor. The load was applied using a load cell with a capacity of 250 kN. A hydraulic jack and a vertical reaction frame system to apply an axial load were used, and three Linear Variation Displacement Transducers (LVDT) of length 100 mm were used to measure the longitudinal shortening displacement and the lateral displacements at mid-length. The columns were vertically positioned, and the upper and lower ends were hinged at a strong frame. The first instrument was the load cell which was used as an indicator of the applied load. It was placed between the top end of the specimen and the bottom end of the hydraulic jack of the testing machine.

The three (LVDT) were placed at three different locations on the steel specimen to measure the longitudinal shortening displacement and the lateral displacements of the upright specimen at various load levels up to failure. (LVDT 1) was used to monitor the longitudinal shortening displacement (ΔZ) of upright. (LVDT 2) and (LVDT 3) were used to monitor the lateral in-plane and out of plane displacements (ΔX, ΔY) at mid-length of upright, where one was placed at the flange and the other at the web. All test data was controlled by a data acquisition system. All experimental tests were carried out at the laboratory of the faculty of engineering at Mattaria- Helwan University. The experimental setup and instrumentations are illustrated in Figure (2).

Preprints (www.preprints.org) | NOT PEER-REVIEWED | Posted: 13 May 2022 doi:10.20944/preprints202205.0176.v1

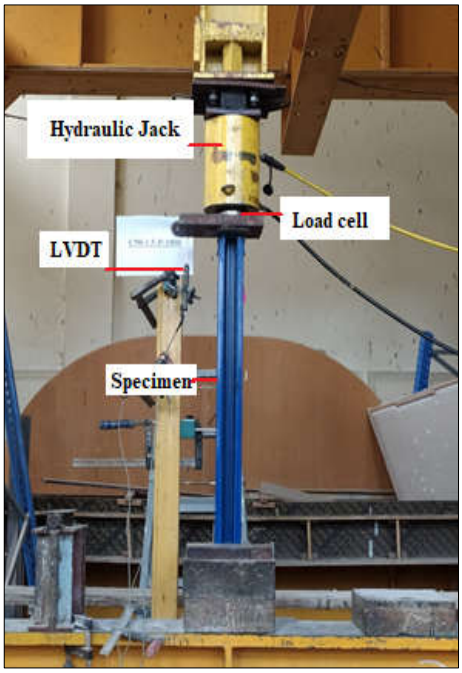

Figure 2. Test set-up and instrumentations.

3. Test Results and Analysis

The axial compression test was carried out experimentally on seventeen perforated specimens with five different cross-sections dimensions and lengths as detailed in Table (1). The results of the ultimate failure load and different deformations of the tested specimens are analyzed as follows:

3.1. Load-displacement curves.

The typical load-axial shortening-displacement (ΔZ) curves of different specimens with different cross-section dimensions and lengths were determined to study the influence of specimen length on the value of ultimate failure load as shown in Figure (3). The relation (P-ΔZ) was compared for the different specimens with the same cross-section but with different slenderness ratios (λ_{max}) according to the variation in lengths. It is obvious that according to the logical concept, the value of the ultimate failure load decreased while shortening-displacement (ΔZ) increased according to the increase in slenderness ratio.

Figure (3) explains that the shortening displacement (ΔZ) for all specimens with lengths 2000mm has a large value than that for specimens with lengths 500 and 1000mm due to the effect of global buckling because the value of the slender ratio increased with the increase in column height.

Preprints (www.preprints.org) | NOT PEER-REVIEWED | Posted: 13 May 2022 doi:10.20944/preprints202205.0176.v1

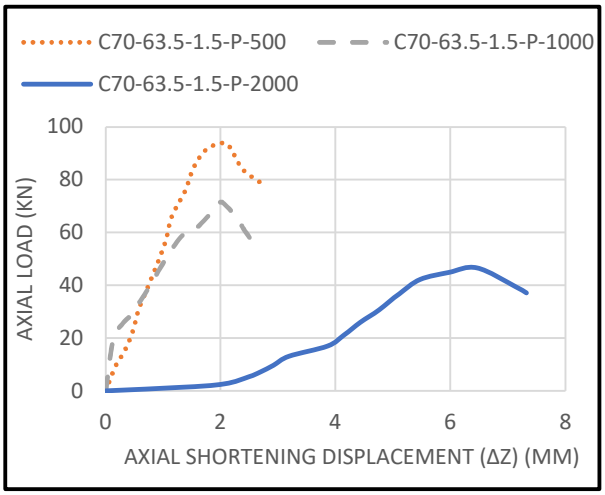

(a) Section type (C70-63.5-1.5-P).

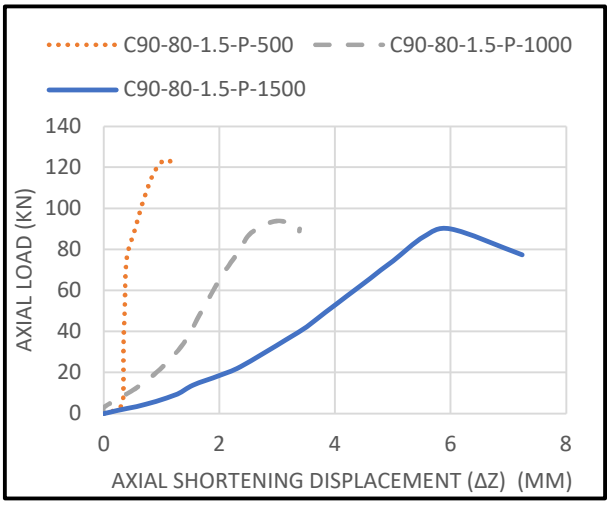

(b) Section type (C90-80-1.5-P)

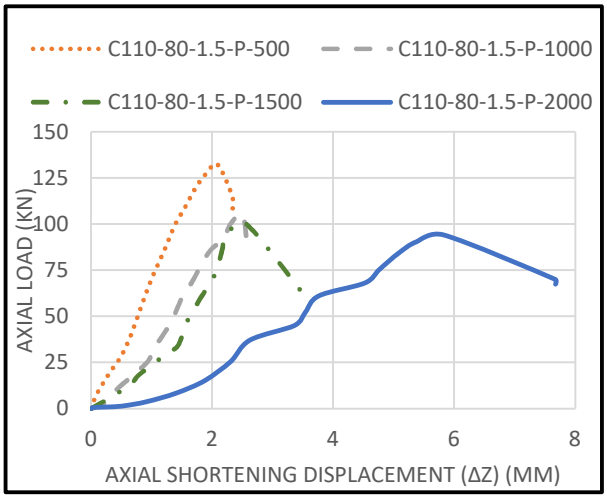

(c) Section type (C110-80-1.5-P).

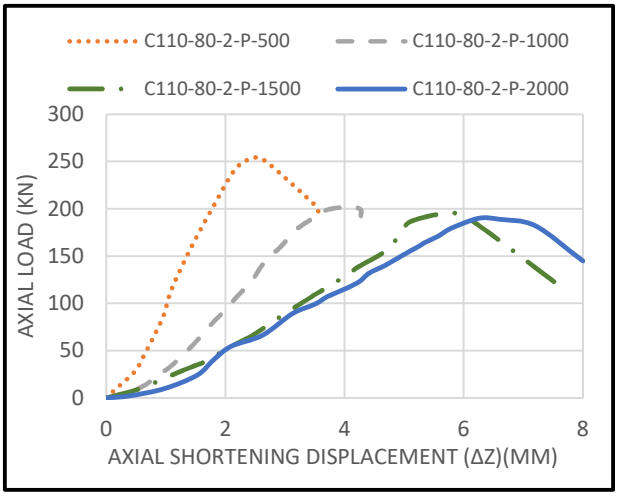

(d) Section type (C110-80-2-P).

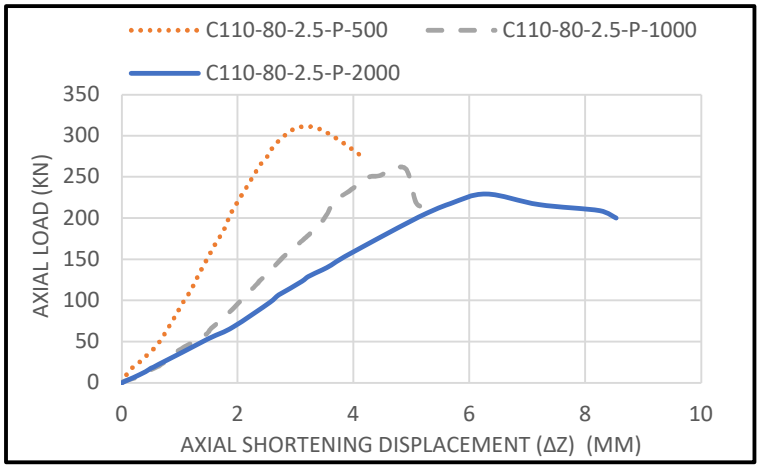

(e) Section type (C110-80-2.5-P).

Figure 3. The load-axial shortening displacement curves.

3.2. Buckling failure modes.

There are different types of failure modes that can affect this type of upright, such as global buckling (GB), distortional buckling (DB), and interaction between distortional

Preprints (www.preprints.org) | NOT PEER-REVIEWED | Posted: 13 May 2022 doi:10.20944/preprints202205.0176.v1

buckling and global buckling (DB+GB) depending on who controls the behavior of the upright, is the critical slenderness ratio or compactness case of its section or both respectively.

The type of buckling failure mode can be determined from the relation between the recorded values of the compression load and corresponding lateral displacements (ΔX) and (ΔY) from (LVDT 2) and (LVDT 3) at the mid-length of each upright for different specimens as shown in Figure (4). The flange displacements, along with very small movement at the web, imply that the distortional buckling (DB) is the main failure mode for the short specimens with lengths equal to 500 and 1000 mm, as shown in Figs. (4-a) to (4-j). This is clearly evident through the pictures of these specimens during the collapse in the laboratory, as shown in Figs. (5-a) to (5-j). Table (3) Shows that the distortional buckling (DB) is the mode of failure for specimens that have a maximum slenderness ratio ($\lambda max <$ 38).

In addition, it is obtained that the distortional-global buckling interaction (DB+GB) dominates the buckling modes of specimens that have a height equal to1500 and 2000 mm with section thickness equal to 1.5 mm such as C90-80-1.5-P-1500, and C110-80-1.5-P-2000 whereas the high value of a maximum slenderness ratio ($38< \lambda max < 75$) with low ratio of compactness as shown in Table (3). Therefore, in this type of specimen, the buckling failure mode is dominated by the interaction of distortionary-global torsional (DB+GB) buckling failure modes, as shown in Figs. (4-k) to (4-p). It is clearly evident through the pictures of these specimens during the collapse in the laboratory, as shown in Figs. (5-k) to (5-m). It is observed that the lateral deformations occur in webs and flanges with approximate equal values and the difference between their values according to the relation between the thickness of the specimen and the value of its maximum slenderness ratio. The increase in the thickness of the cross-section decreases the effect of distortion as shown in Figures (4-m), (4-o), and (4-p), where specimens C110-80-2-P-2000 and C110-80-2.5-P-2000 have almost the same displacements of webs and flanges for each specimen. So that this type of specimen, is mostly governed by the effect of global-buckling (GB) higher than that for distortional buckling (DB), and then the cross-section shape remains non-deformable when buckling occurs and the effect of distortion is small. Therefore, the collapse of specimen C70-63.5-1.5-P-2000 occurred due to the effect of global-buckling (GB) alone as shown in Figure (5-n) because according to the classification of ECP, this section is non-compact, and the maximum slenderness ratio is high ($\lambda max \geq 89.5$). Figure (4-q) shows that the lateral deformations for the web and flanges of this specimen are closely equal.

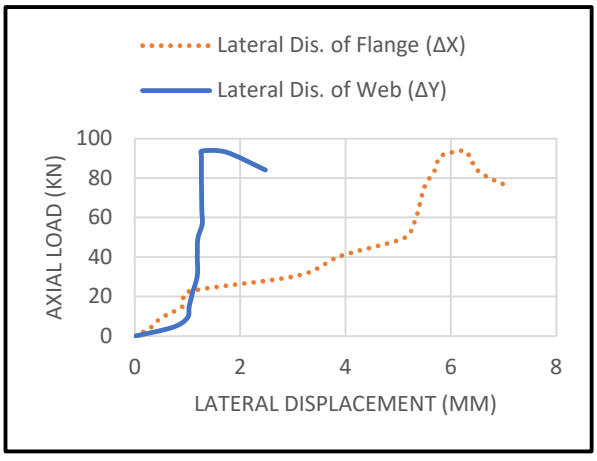

(a) C70-63.5-1.5-P-500.

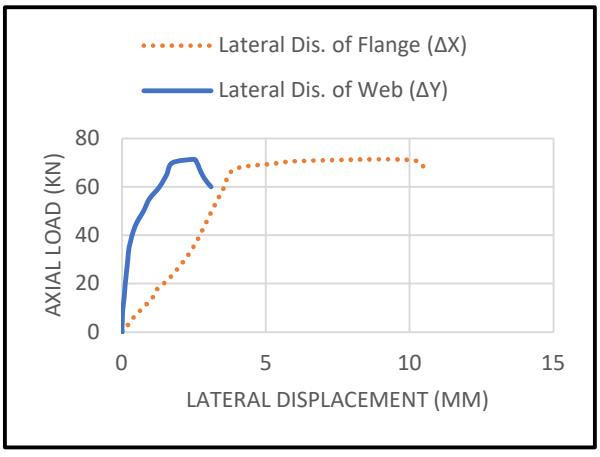

(b) C70-63.5-1.5-P-1000.

Preprints (www.preprints.org) | NOT PEER-REVIEWED | Posted: 13 May 2022 doi:10.20944/preprints202205.0176.v1

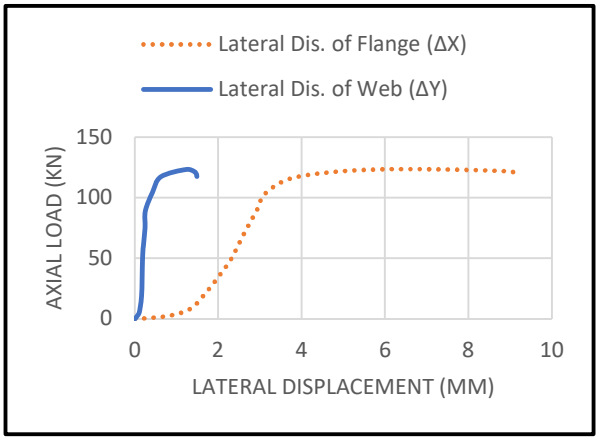

(c) C90-80-1.5-P-500.

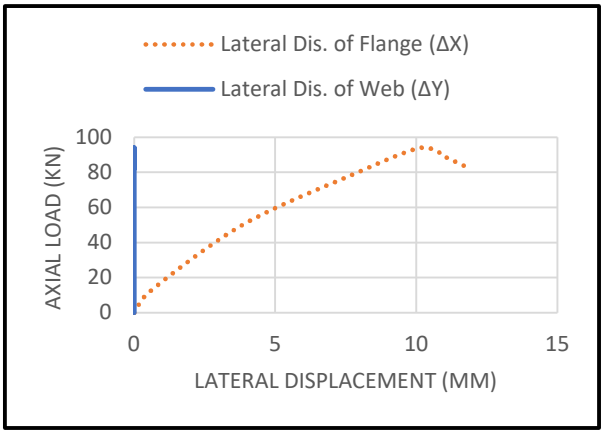

(d) C90-80-1.5-P-1000.

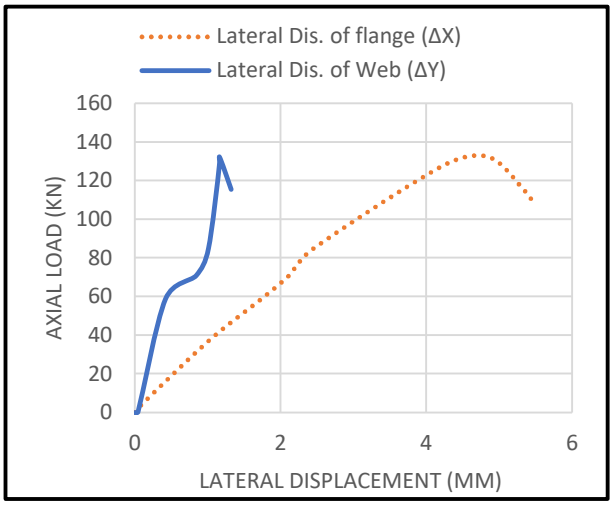

(e) C110-80-1.5-P-500.

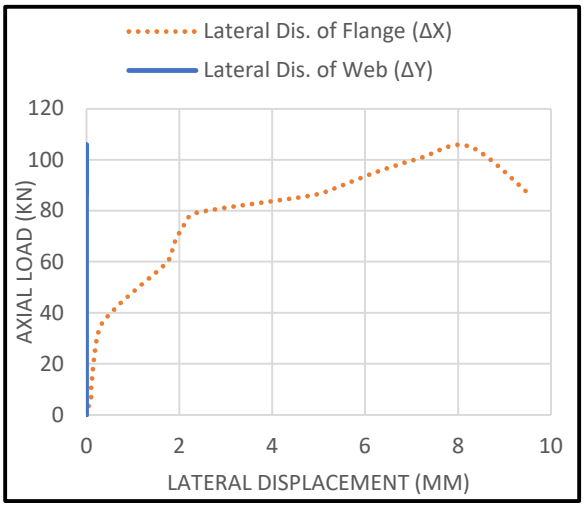

(f) C110-80-1.5-P-1000.

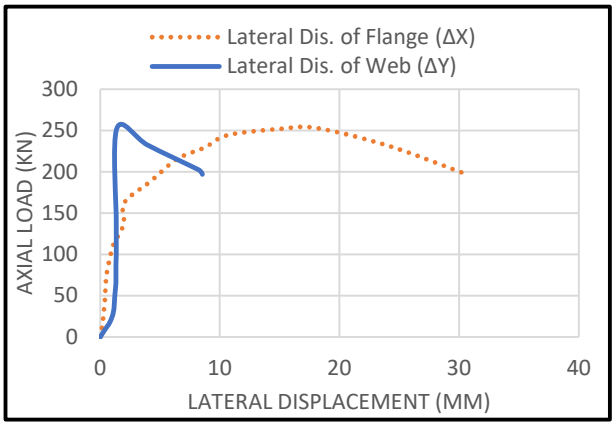

(g) C110-80-2-P-500.

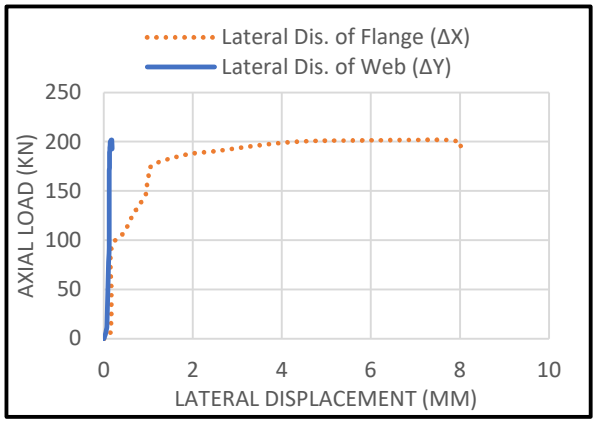

(h) C110-80-2-P-1000.

Preprints (www.preprints.org) | NOT PEER-REVIEWED | Posted: 13 May 2022 doi:10.20944/preprints202205.0176.v1

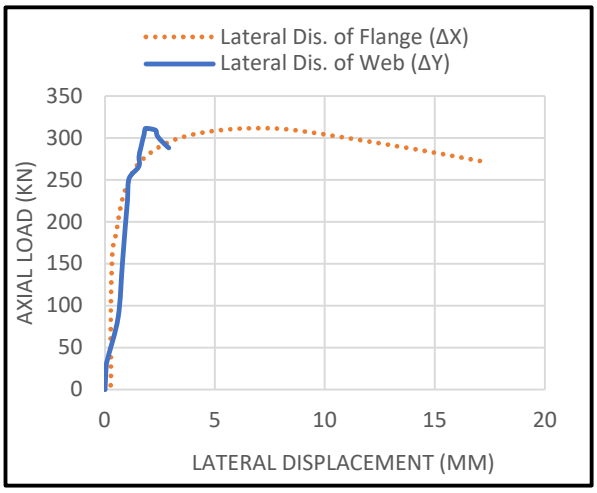

(i) C110-80-2.5-P-500.

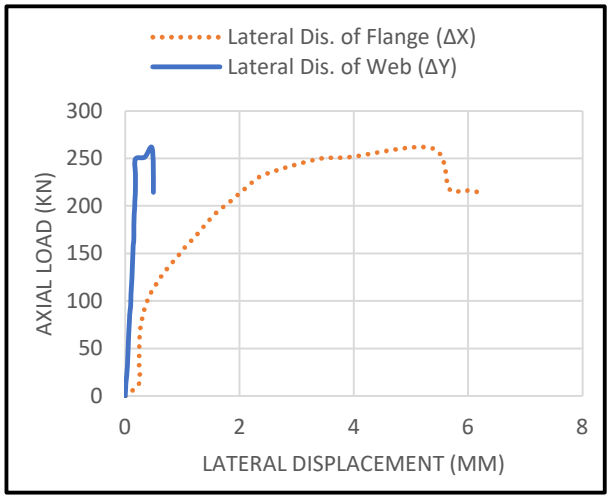

(j) C110-80-2.5-P-1000.

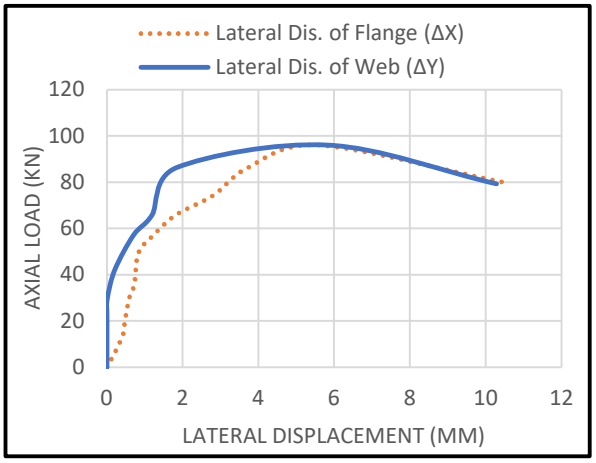

(k) C90-80-1.5-P-1500.

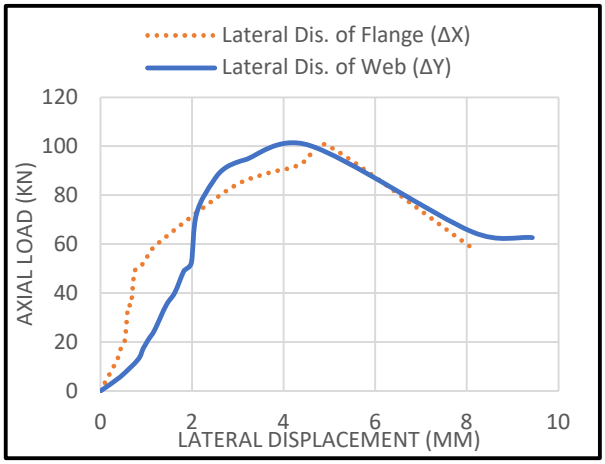

(l) C110-80-1.5-P-1500.

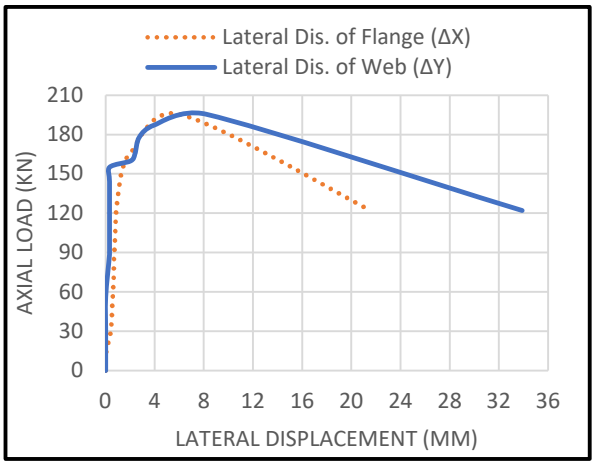

(m) C110-80-2-P-1500.

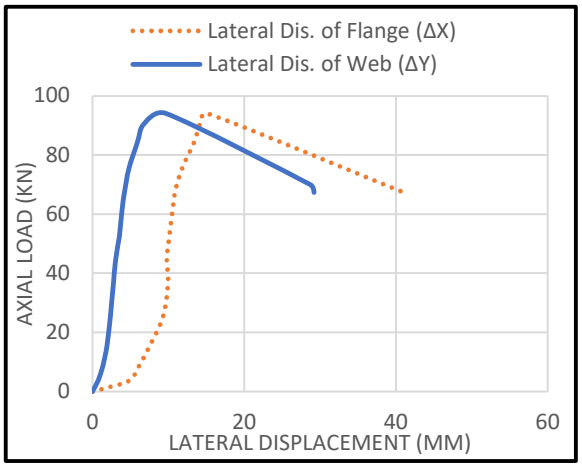

(n) C110-80-1.5-P-2000

Preprints (www.preprints.org) | NOT PEER-REVIEWED | Posted: 13 May 2022 doi:10.20944/preprints202205.0176.v1

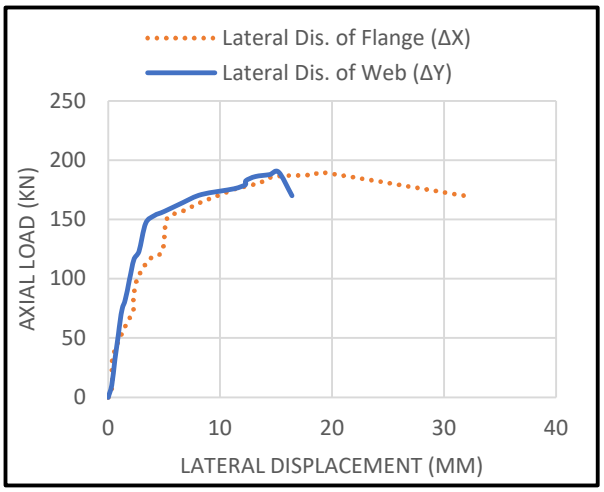

(o) C110-80-2-P-2000.

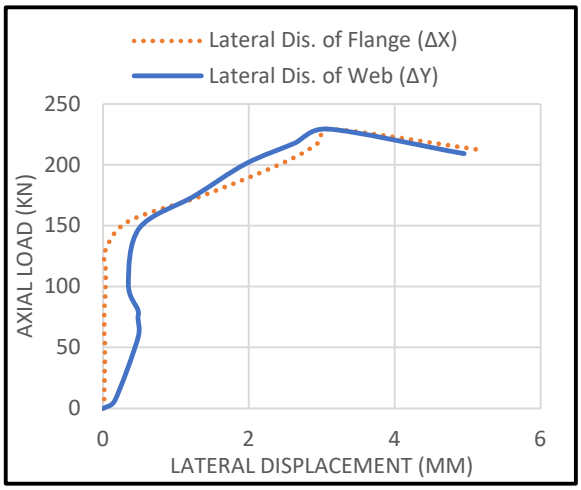

(p) C110-80-2.5-P-2000.

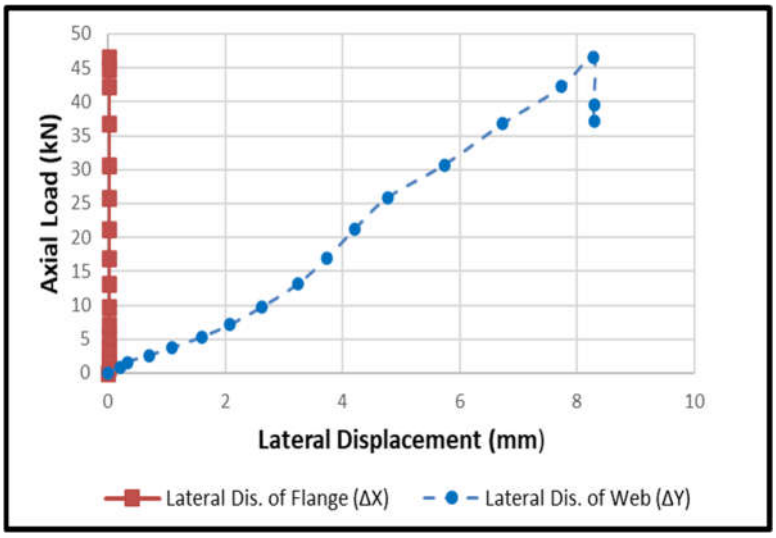

(q) C70-63-1.5-P-2000.

Figure 4. The load-lateral displacement curves according to the experimental test for different specimens.

Preprints (www.preprints.org) | NOT PEER-REVIEWED | Posted: 13 May 2022 doi:10.20944/preprints202205.0176.v1

Table 3. Ultimate loads, normalized strength, and failure modes.

Specimen	λ_{max}	$P_y = F_y * A_{net}$ (kN)	$P_{u,(exp)}$ (kN)	$\frac{P_{u,(exp)}}{P_y}$	Failure mode
C70-63.5-1.5-P-500	22.38	125.3	93.6	0.75	(DB)
C70-63.5-1.5-P-1000	44.76	125.3	71.4	0.57	(DB)
C70-63.5-1.5-P-2000	89.52	125.3	46.6	0.37	(GTB)
C90-80-1.5-P-500	18.51	158.17	123.5	0.78	(DB)
C90-80-1.5-P-1000	37.02	158.17	93.8	0.6	(DB)
C90-80-1.5-P-1500	55.54	158.17	90.1	0.57	(DB+GB)
C110-80-1.5-P-500	18.54	179.72	132.3	0.74	(DB)
C110-80-1.5-P-1000	37.09	179.72	105.3	0.59	(DB)
C110-80-1.5-P-1500	55.63	179.72	100.4	0.56	(DB+GB)
C110-80-1.5-P-2000	74.18	179.72	94.1	0.53	(DB+GB)
C110-80-2-P-500	18.61	245.28	253	1.03	(DB)
C110-80-2-P-1000	37.22	245.28	201.9	0.82	(DB)
C110-80-2-P-1500	55.82	245.28	195.6	0.8	(DB+GB)
C110-80-2-P-2000	74.43	245.28	190.1	0.77	(DB+GTB)
C110-80-2.5-P-500	18.67	305.96	311.5	1.02	(DB)
C110-80-2.5-P-1000	37.34	305.96	260.8	0.86	(DB)
C110-80-2.5-P-2000	74.68	305.96	229.5	0.75	(DB+GTB)

(a) C70-63.5-1.5-P-500 (DB)

(b) C90-80-1.5-P-500 (DB)

(c) C110-80-1.5-P-500 (DB)

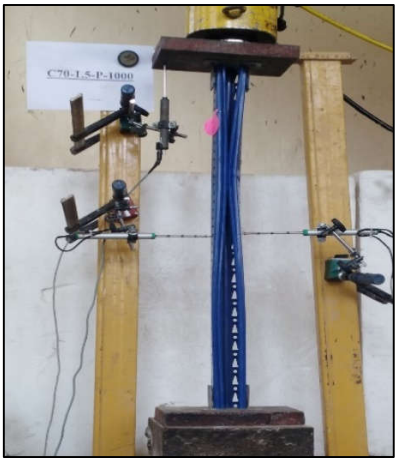

Preprints (www.preprints.org) | NOT PEER-REVIEWED | Posted: 13 May 2022 doi:10.20944/preprints202205.0176.v1

(d) C110-80-2-P-500 (DB) (e) C110-80-2.5-P-500 (DB) (f) C70-63.5-1.5-P-1000 (DB)

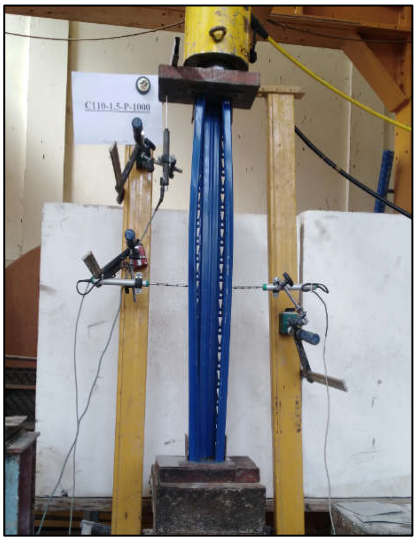

(g) C110-80-1.5-P-1000 (DB) (h) C110-80-2-P-1000 (DB) (i) C110-80-2.5-P-1000 (DB)



(j) C90-80-1.5-P-1000 (DB) (k)C110-80-2-P-2000 (DB+GTB) (l) C110-80-2.5-P-2000 (DB+GTB).

Preprints (www.preprints.org) | NOT PEER-REVIEWED | Posted: 13 May 2022 doi:10.20944/preprints202205.0176.v1


(m) C110-80-1.5-P-2000 (DB+GB)

(n) C70-63.5-1.5-P-2000 (GB)

Figure 5. The pictures of the different specimens at the collapse during the experimental test.

3.3. The normalized ultimate compression strength ratio.

The normalized ultimate compression strength ratio is the ratio between the maximum value of axial failure load which was determined from the experimental test (Pu,exp), and the axial yield load (Py) for each specimen as shown in Table (3). It can be used as a good reference to determine the efficiency of benefit from upright members according to the appropriateness of its cross-section's dimensions to the value of slenderness ratio. Therefore, the higher the normalized ultimate compression strength ratio, the better the dimensions of the cross-section to the value of slenderness ratio, and vice versa.

Table (3) shows that the values of the normalized ultimate compression strength ratio (Pu,exp./Py) for all specimens ranged from 0.37 to 1.03 according to the value of the slenderness ratio and the compactness ratio.

4. Comparison between direct strength method and experimental test

The Direct Strength Method (DSM) has become very popular due to its simplicity, it has been accepted in codes of cold-formed steel design such as North American specification AISI-S100 [14] and the Australian/New Zealand standard AS/NZS4600 [15]. Many researchers working in the subject of thin-walled constructions use it. The DSM is now fully incorporated in the current versions of AISI-S100 as an alternative design technique for cold-formed steel structures.

The applicability of utilizing the DSM to estimate the ultimate strength of uprights failing in various buckling modes is investigated in this section. The following are the equations for the DSM method:

$$P_{DSM} \text{ is the nominal axial strength} = \text{min. of} \begin{cases} P_{ne} \\ P_{nd} \\ P_{nl} \end{cases} \quad (1)$$

Where P_{ne}: is the nominal axial strength in case of global buckling failure.

$$P_{ne} = \begin{cases} (0.658)^{\lambda_c^2} P_y & \text{for } \lambda_c \leq 1.5 \\ \left(\frac{0.877}{\lambda_c^2}\right) P_y & \text{for } \lambda_c > 1.5 \end{cases} \quad (2)$$

Preprints (www.preprints.org) | NOT PEER-REVIEWED | Posted: 13 May 2022 doi:10.20944/preprints202205.0176.v1

Where $\lambda_c = \sqrt{P_y / P_{cre}}$, $P_y = Af_y$, P_{nd}: is the nominal axial strength in case of distortional buckling failure.

$$P_{nd} = \begin{cases} P_y & \text{for } \lambda_d \leq 0.561 \\ \left(1 - 0.25\left(\frac{P_{crd}}{P_y}\right)^{0.6}\right)\left(\frac{P_{crd}}{P_y}\right)^{0.6} P_y & \text{for } \lambda_d > 0.561 \end{cases} \quad (3)$$

Where $\lambda_d = \sqrt{P_y / P_{crd}}$, P_{nl}: is the nominal axial strength in case of local buckling failure.

$$P_{nl} = \begin{cases} P_{ne} & \text{for } \lambda_l \leq 0.776 \\ \left(1 - 0.15\left(\frac{P_{crl}}{P_{ne}}\right)^{0.4}\right)\left(\frac{P_{crl}}{P_{ne}}\right)^{0.4} P_{ne} & \text{for } \lambda_l > 0.776 \end{cases} \quad (4)$$

Where $\lambda_l = \sqrt{P_{ne} / P_{crl}}$, λ_c, λ_d, and λ_l : are the slenderness factors for overall, distortional, and local buckling, respectively. P_y : is the squash load of a cross-section. [Pcr,e], [Pcr,d], and [Pcr,l] are the critical elastic load due to overall global, distortional, and local buckling, respectively. The DSM is used to estimate the values of the ultimate axial strength and the type of failure modes of the stiffened perforated cold-formed steel uprights with different geometries and the results are compared with that determined from the experimental tests as shown in Table 4.

Table 4. Comparison of test strengths with DSM strengths.

Specimen	$P_{u,exp}$ (kN)	$P_{n,DSM}$ (kN)	$P_{n,DSM.}/ P_{u,exp}$	Experimental Failure mode	DSM Failure mode
C70-63.5-1.5-P-500	93.6	112.1	1.2	DB	LB
C70-63.5-1.5-P-1000	71.4	100.9	1.4	DB	LB
C70-63.5-1.5-P-2000	46.6	32.9	0.7	GTB	LB
C90-80-1.5-P-500	123.5	145.2	1.2	DB	LB
C90-80-1.5-P-1000	93.8	138.6	1.5	DB	LB
C110-80-1.5-P-500	132.3	163.1	1.2	DB	LB
C110-80-1.5-P-1000	105.3	125.87	1.2	DB	LB
C110-80-1.5-P-2000	94.1	98.38	1.04	DB+GB	LB
C110-80-2-P-500	253	209.26	0.8	DB	LB
C110-80-2-P-1000	201.9	180.40	0.9	DB	LB
C110-80-2-P-2000	190.1	132.3	0.7	DB+GTB	LB
C110-80-2.5-P-500	311.5	272.7	0.9	DB	LB
C110-80-2.5-P-1000	260.8	228.67	0.9	DB	LB
C110-80-2.5-P-2000	229.5	183.71	0.8	DB+GTB	LB

From Table 4 it is observed that the failure mode predicted by the DSM was only the local buckling for all specimens. While, according to the experimental tests the mode of failure may be global buckling, distortional buckling, or interaction between distortional and global buckling dependent on the geometrical, the specimen cross-section dimensions, and the value of its slenderness ratio. That means the DSM is not able to provide the interactive failure modes prediction. The perforated steel storage rack uprights subjected to axial compression evaluated in this paper have complex cross-sections that are

Preprints (www.preprints.org) | NOT PEER-REVIEWED | Posted: 13 May 2022 doi:10.20944/preprints202205.0176.v1

not specified in the Direct Strength Method (DSM) provided in the North American Specification (AISI S100) [13].

Figures (6-a) and (6-b) show the comparison between the results of the experimental test and DSM for distortional and global strength respectively. It is seen that the distortional buckling curve of the DSM is generally overestimated by the predictions of distortional and distortion-global buckling failure obtained from the experimental tests. Furthermore, for distortional-global buckling interaction failures, the experimental test predictions show that some specimens are below, and some are above the DSM's global buckling strength curve.

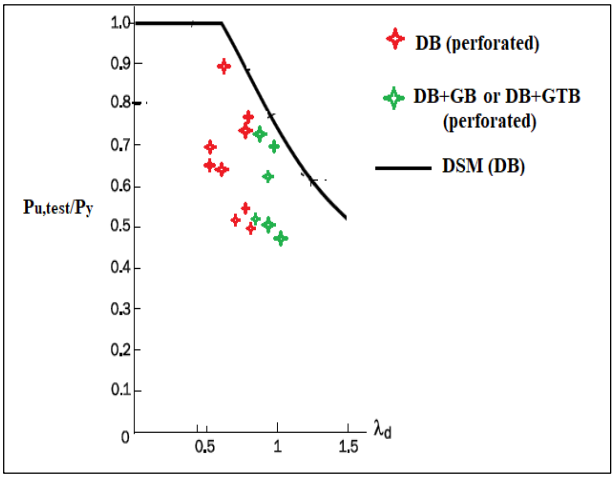

(a) DSM distortional strength curve and experimental results

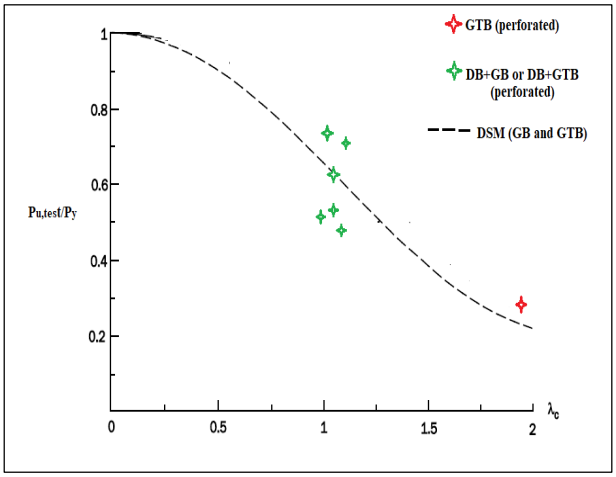

(b)DSM global strength curve and experimental results.

Figure 6. Comparison between the results of DSM and the results of the experimental test.

The current DSM distortional buckling strength curve and global buckling strength curve do not offer a reliable design for stiffened perforated steel storage rack uprights subjected to axial compression because the presence of perforations significantly affects the behaviour and failure buckling modes, as shown in Table 4. The ultimate strength obtained from tests and predicated on DSM may be incompatible as shown in Table 4. Xianzhong Zhao etc. al. [2] developed a modified DSM distortional buckling strength curve to be used for perforated uprights as detailed in the following equations:

$$P_{nd} = \begin{cases} P_{ynet} & for\ \lambda_d \le \lambda_{d1} \\ P_{ynet} - \left[\frac{P_{ynet}-P_{d2}}{\lambda_{d2}-\lambda_{d1}}\right](\lambda_d - \lambda_{d1}) & for\ \lambda_{d1} < \lambda_d \le \lambda_{d2} \end{cases} \quad (5)$$

Where: $\lambda_d = \sqrt{P_y / P_{crd}}$, $\lambda_{d1} = 0.561\, P_{ynet}/P_y$, $\lambda_{d2} = 0.561\left[14\left(\frac{P_y}{P_{ynet}}\right) - 13\right]$, $P_{d2} = \left[1 - 0.25\left(\frac{1}{\lambda_{d2}}\right)^{1.2}\right]\left(\frac{1}{\lambda_{d2}}\right)^{1.2} P_y$, P_{crd} is the Critical elastic buckling load (first buckling mode), $P_{y,\,net} = A_{net} * F_y$, where A_{net} is the net cross-sectional area.

Figure 7 shows the comparison between the results of the modified DSM distortional strength curve and the experimental test results. It is observed that the results of the two methods are close.

Preprints (www.preprints.org) | NOT PEER-REVIEWED | Posted: 13 May 2022 doi:10.20944/preprints202205.0176.v1

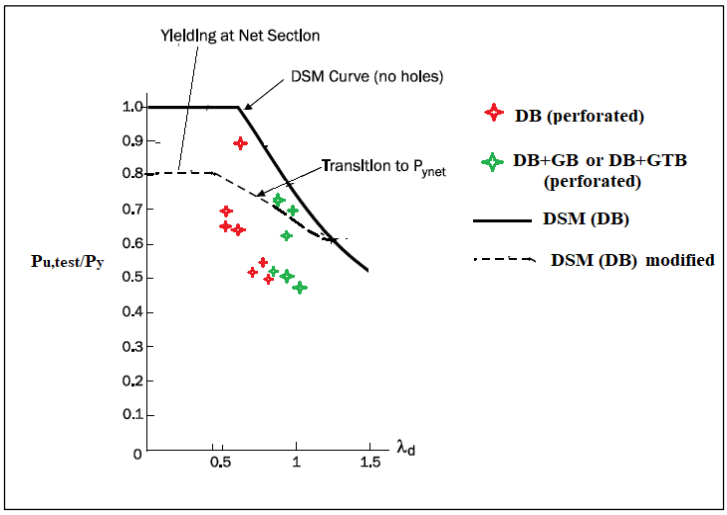

Figure 7. Comparison between the modified DSM distortional strength curve experimental test results.

5. Conclusions

This paper has presented an experimental investigation into the behavior of stiffened perforated cold-formed steel sections subjected to axial compression. A total of seventeen experimental results were reported. The material properties were determined from the tensile coupon tests. Experimental tests were carried out to observe the buckling failure modes. Axial compression capacity, load-axial shortening, and load-lateral displacement relationships are discussed. The effect of the upright total lengths, the overall web height of cross-sections, and the thickness was investigated. Based on the experimental results presented in this paper, the following conclusions are drawn:

- The distortional buckling (DB) is the mode of failure for specimens that have a maximum slenderness ratio ($\lambda_{max} < 38$)
- The distortional-global buckling interaction (DB+GB) dominates the buckling modes of specimens that have a height equal to1500 and 2000 mm with section thickness equal to 1.5 mm whereas the high value of a maximum slenderness ratio ($38 < \lambda max < 75$) with low ratio of compactness.
- The collapse of the specimen occurred due to the effect of global-buckling (GB) alone when the maximum slenderness ratio is high ($\lambda_{max} \geq 89.5$) and the section is classified as a non-compact section.
- The value of the normalized ultimate compression strength ratio ($P_{u,exp./}P_y$) for all specimens ranged from 0.37 to 1.03 according to the value of the slenderness ratio and the compactness ratio. It is smaller than unity for all specimens unless that has maximum slenderness ratio is small ($\lambda_{max} \leq 18.7$) and the section is classified as a non-compact section.
- The web height has a marginal effect on the percentage of increase in ultimate axial compression capacity when the web increases from 90 mm to 110 mm compared to the percentage of increase in cross-section area, for all lengths. This is attributed to the percentage increase in ultimate capacity ranging from 7.1% to 12.2% and less than the percentage increase in cross-section area, which equals 13.6%.
- The web-thickness ratio is the major factor influencing the ultimate axial compression capacity. When the web height is constant and increased of the plate thickness, then the web-thickness ratio decreases, and the ultimate axial compression capacity increases, for all specimens' lengths.
- The results of this study explicitly show that the Direct Strength Method (DSM) has been demonstrated to be unreliable for predicting the ultimate strength of uprights failing in buckling interactions for perforated uprights.

 doi:10.20944/preprints202205.0176.v1

- The failure modes of perforated specimens with stiffeners generally cannot be well predicted by the Direct Strength Method.
- The findings of this study clearly reveal that the Direct Strength Method (DSM) modification carried out by Xianzhong Zhao etc. al. has been shown to be reliable for forecasting the ultimate strength of uprights failing in buckling interactions for perforated uprights.

6. Patents

This section is not mandatory but may be added if there are patents resulting from the work reported in this manuscript.

Supplementary Materials: None.

Author Contributions: Conceptualization, Methodology, Fattouh; software, Yehia; data curation,.Mamdouh; supervision, Deifalla.

Funding: This research received no external funding.

Data Availability Statement: Not applicable.

Acknowledgments: Not applicable

Conflicts of Interest: The authors declare no conflict of interest.

References

1. Casafont, M., Pastor, M., Roure, F. and Pekoz, T. (2011), "An experimental investigation of distortional buckling of steel storage rack columns", Thin-Walled Structures, 49(8), 933–946.
2. Xianzhong Zhao, Chong Ren, and Ru Qin. (2017), "An experimental investigation into perforated and non-perforated steel storage rack uprights", Thin-Walled Structures, 112, 159–172.
3. Rhodes, J. and Schneider, F. (1994), "The compressional behavior of perforated elements", CCFSS Proceedings of International Specialty Conference on Cold-Formed Steel Structures 6.
4. Crisan, A., Ungureanu, V. and Dubina, D. (2012), "Behaviour of cold-formed steel perforated sections in compression. Part 1—Experimental investigations", Thin-Walled Structures, 61, 86–96.
5. EN 15512, (2020), "The European standard for steel static storage systems - Adjustable pallet racking systems", European standards.
6. Roure, F., Pastor, M., Casafont, M. and Somalo, M. (2011), "Stub column tests for racking design: experimental testing, FE analysis, and EC3", Thin-Walled Structures, 49(1), 167–184.
7. KS. Sivakumaran, (1987), "Load capacity of uniformly compressed cold-formed steel section with punched web", Canadian Journal of Civil Engineering. 14(4).
8. Moen, CD. and Schafer, B.W. (2008), "Experiments on cold-formed steel columns with holes", Thin-Walled Structures, 46(10), 1164–1182.
9. Banwait, AS. (1987), "Axial load behavior of thin-walled steel sections with openings", PhD thesis; Department of Civil and Environmental Engineering, Mc.Master University, Hamilton, Ontario.
10. Baldassino, N. and Hancock, G. (1999), "Distortional buckling of cold-formed steel storage rack sections including perforations", 4th Int. Conf. on Steel and Aluminum Structures.
11. Kwon, YB., Kim, BS. and Hancock, GJ. (2009), "Compression tests of high strength cold-formed steel channels with buckling interaction", J. Constr. Steel Res. 65(2), 278–289.
12. Xiang, Y., Zhou, X., Shi, Y., Xu, L. and Xu, Y. (2020), "Experimental investigation and finite element analysis of cold-formed steel channel columns with complex edge stiffeners", Thin-Walled Structures, 152, 106-120.
13. Schafer, B. W., and Peköz, T. (1998). "Computational modeling of cold-formed steel: characterizing geometric imperfections and residual stresses." Journal of Constructional Research, 47, 193-210.
14. AISI-S100. (2016). North American Specification for the Design of Cold-Formed Steel Structural Members, American Iron, and Steel Institute, Washington, D.C.
15. AS/NZS4600 (2018). Cold-formed steel structures. Standards Australian/New Zealand, Wellington; 2018
16. C. D. Moen and B. W. Schafer, "Elastic buckling of cold-formed steel columns and beams with holes," Engineering Structures, vol. 31, no. 12, pp. 2812–2824, 2009.
17. X. Yao, Y. Guo, Y. Liu et al., (2020) "Analysis on distortional buckling of cold-formed thin-walled steel lipped channel steel members with web openings under axial compression," Indian Concrete Journal, vol. 50, No. 1, pp. 170–177, In Chinese.